

EXTREME COMPRESSION OF HEAVY-ION BEAM PULSES: EXPERIMENTS AND MODELING *

A. B. Sefkow¹, R. C. Davidson¹, P. C. Efthimion¹, E. P. Gilson¹, I. D. Kaganovich¹,
J. E. Coleman², P. K. Roy², P. A. Seidl², J. J. Barnard³, D. R. Welch⁴,
¹PPPL, ²LBNL, ³LLNL, and ⁴Voss Scientific, USA

Abstract

Longitudinal bunch compression of intense ion beams for warm dense matter and heavy ion fusion applications occurs by imposing an axial velocity tilt onto an ion beam across the acceleration gap of a linear induction accelerator, and subsequently allowing the beam to drift through neutralizing plasma as the pulse compresses. The finite-size of the acceleration gap and time-dependent nature of the induction voltage waveform for longitudinal compression are demonstrated to increase the effective longitudinal temperature of the charge bunch, reduce the resulting fractional velocity tilt from its intended value, and transversely defocus the beam in a time-dependent manner. The over-focusing technique or a strong final-focus solenoid may be used to refocus the longitudinally compressing beam to the small spot size required (sub-mm to few mm) at a coincident focal plane. In the case of a final-focus solenoid, supersonic cathodic-arc plasma may be injected into the high-field region from the low-field end for beam neutralization experiments.

INTRODUCTION

Of the challenges encountered in developing heavy ion drivers [1] for warm dense matter and heavy ion fusion applications [2], one of the most significant is found in the final transport section leading to the target, where ion beam compression in space and time is required in order to achieve the necessary high intensities for striking the target [3,4]. In other words, intense ion beam pulses must undergo simultaneous transverse and longitudinal bunch compression to a coincident focal plane in order to meet the requisite beam power on target [5]. Heavy ion drivers can deliver more intensity to the target per unit length of accelerator by greatly compressing intense ion charge bunches.

The Neutralized Transport Experiment [6] has demonstrated the feasibility of transverse compression of an intense charge bunch by applying a radial focusing angle to the beam prior to neutralizing its space-charge and current in a plasma-filled drift region. When the plasma density n_p is much larger than the beam density n_b throughout the drift region, quasineutrality is maintained and the beam focuses ballistically to a small radius r_b (few mm). When the neutralization level is very high, the focusing is emittance-dominated, meaning only the inherent temperature of the beam T_b limits the final beam

radius, due to chromatic aberration.

The Neutralized Drift Compression Experiment (NDCX) [7] currently studies longitudinal compression in a similar way, by providing plasma to neutralize the beam as it focuses in the axial direction. The primary component upgrade to the previous experiment is a linear induction accelerator with one acceleration gap, which is also known as an induction module. The induction module employs a time-dependent voltage waveform $V(t)$ to modify the axial velocity v_z profile of the beam, in order to decrease the initial pulse length t_p and increase the current of the beam. Such longitudinal focusing can also be emittance-dominated, provided that the accuracy of the imposed velocity tilt and the level of neutralization by the plasma are both high. The figures of merit are the compression ratio (maximum final to initial current) and the minimum full-width, half-maximum pulse duration t_{fwhm} at focus. Compression ratios greater than 50 with full-width, half-maximum pulse lengths < 5 ns have been measured [8] in the NDCX device, and agree well with reduced numerical models and simulations [9]. Upcoming experiments will attempt to transversely focus a beam with an axial velocity tilt to a sub-mm spot size at a coincident focal plane. Particle-in-cell (PIC) simulations [5] and future experiments [10] seek to optimize the amount of current density compression, for a given set of experimental constraints.

ACCELERATION GAP EFFECTS AND ABERRATION

There exists an ideal induction module voltage waveform $V(t)$ that results in the imposition of a perfect velocity tilt on an ion beam with zero temperature, across an infinitely thin acceleration gap, for achieving maximal longitudinal compression at a desired focal plane [11]. In the classical limit of point particles, there is no upper bound on the longitudinal current compression (or lower bound on the pulse length) under the assumptions mentioned. In reality, current compression cannot be infinite due to physical constraints that ultimately limit the achievable compression factors and pulse lengths [12].

Making the assumptions that the initial beam energy E_0 entering the gap is constant in time and that equal amounts of head and tail are decelerated and accelerated, respectively, allows the head and tail velocities to be defined as $v_h = v_0 (1-f/2)$ and $v_t = v_0 (1+f/2)$, respectively, where v_0 is the initial velocity of the beam before entering the gap, and the fractional velocity tilt f is defined as $f = \Delta v/v_0 = (v_t - v_h)/v_0$. Then, the time and drift length to

*This research was supported by the U.S. Department of Energy under the auspices of the Heavy Ion Fusion Science Virtual National Laboratory.

longitudinal focus are [13] $t_b^{\text{foc}} = [(1/f)+(1/2)] t_p$ and $L_d = v_0 [(1/f)-(f/4)] t_p$, where t_p is the initial pulse length of the beam, which is usually written as $t_p = L_b/v_0$, where L_b is the initial bunch length. For the same E_0 , larger tilts f give shorter L_d than smaller tilts, and longer initial pulse lengths t_p give longer L_d than shorter pulse lengths.

The ideal time dependence of the velocity as the axially compressing beam exits the acceleration gap is

$$v_b(t) = v_0 (1-f/2) / \{1-[f/(1+f/2)](t/t_p)\},$$

where t is evaluated from $t = 0$ to $t = t_p$. Then, the required ideal voltage waveform $V(t)$ to time-dependently alter the beam energy across the infinitely thin gap is given by [11]

$$V(t) = (m_b v_0^2 / 2q_b) \{[(1-f/2) / \{1-[f/(1+f/2)](t/t_p)\}]^2 - 1\},$$

where m_b and q_b are the beam particle mass and charge, respectively, and t is evaluated from $t = 0$ to $t = t_p$.

Realistically, an ion beam created in the laboratory must encounter a finite-size gap, always has some finite temperature, and might not be entirely monoenergetic entering the gap (or have the appropriate energy for the imparted voltage waveform). In experiments, the induction module is programmed to attempt the application of as near an ideal waveform as possible. However, the induced electric field encountered by the beam has significant spatial and temporal extent, relative to the bunch and pulse lengths of the beam, rather than modifying the beam energy over an infinitely thin slice.

Sets of particle-in-cell (PIC) simulations are executed in order to quantitatively assess and classify the origin of different sources of longitudinal focal plane degradation involving the 3 cm-long acceleration gap in NDCX [13]. All of the PIC simulations presented in this paper are executed with the LSP code [14]. In general, ion beam trajectories must be evaluated numerically by PIC techniques in order to take into account many of the effects that ultimately determine the quality of the focal plane, and there is no universally valid analytical model for determining the expected current compression at the focal plane.

In order to ascertain the effects of the finite-size acceleration gap in the NDCX on the longitudinal beam dynamics, two types of induction module voltage waveform are studied across the experimental 3 cm gap, which is centered at $z = -20.5$ cm in this coordinate system (the axial coordinate extends from $z = -30$ cm to $z = +100-250$ cm, depending on the drift length, where $z = 0$ is the approximate starting location of the plasma). They are called the “sharp” and “smooth” waveforms and are illustrated in Fig. 1 [$V(t) > 0$ results in an $-E_z(z)$ in this model]. The $V(t)$ shown corresponds to the ideal waveform for an $E_0 = 400$ keV K^+ beam with an intended $f = 0.5$ over the initial $t_p = 300$ ns, from $t = 200$ ns to $t = 500$ ns. The drift length to the longitudinal focal plane is calculated to be $L_d \sim 78.7$ cm ($z \sim +58.2$ cm).

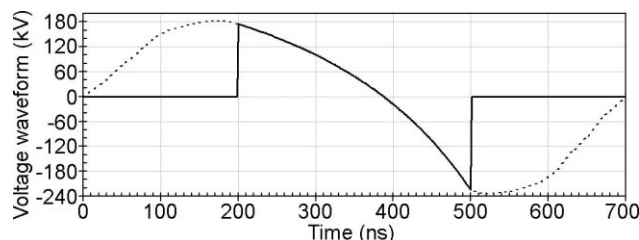


Fig. 1. Representative “sharp” (solid line) and “smooth” (dashed line) $V(t)$ voltage waveforms used in simulations.

The “sharp” waveform ensures that only the ideal electric field is imposed for the duration of the beam’s initial pulse length. However, the experimentally realizable waveform requires ramp-up and ramp-down time for its voltage swing, and results in a waveform akin to the “smooth” one. Simulations comparing both waveforms shed insight into the contribution to the longitudinal focusing dynamics from the suspected non-ideal extra voltage present in the “smooth” waveform.

The initial cold K^+ beam parameters are $E_0 = 400$ keV, $t_p = 300$ ns, and $T_b = 0$ eV (corresponding to no emittance). The induced electric field varies as a function of space and time according to the boundary conditions and the applied “sharp” waveform in the gap, respectively. The cold beam suffers compression degradation compared to an ideal gap case: the compression ratio reduces to 2200 (from infinity), and the t_{fwhm} increases to 0.03 ns (from zero), as a sole result of the finite-size gap. When the “sharp” $V(t)$ is exchanged with the more realistic “smooth” waveform, a significant difference in the $\{z, v_z\}$ phase space of the beam is witnessed, as shown in Fig. 2 at $t = 820$ ns (the time to focus is $t \sim 959$ ns, and the initial $t_p > 300$ ns). Decompressing portions of the charge bunch precede and follow the compressing region. Differences in shape are solely due to the presence of the extra voltage from the finite rise-time and fall-time of the “smooth” waveform.

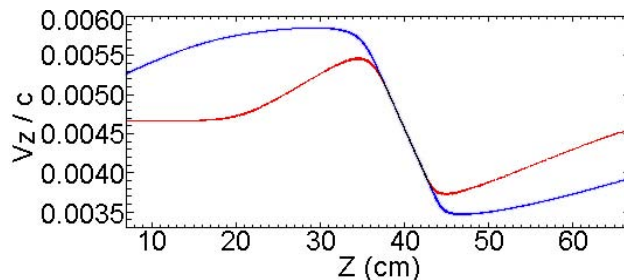


Fig. 2. $\{z, v_z\}$ phase space at $t = 820$ ns for the $T_b = 0$ eV beam after application of the “sharp” (red) and “smooth” (blue) $V(t)$ waveforms.

The transit time of the beam particles across the finite-size gap (~ 75 ns for a 400 keV K^+ ion because of the effective $\Delta z \sim 10$ cm spatial extent of E_z from the 3 cm gap at $r_w = 3.8$ cm) is an important consideration, since it causes the particles to sample a significant temporal range of the voltage waveform. The integrated force over the gap is less than the intended amount to achieve the

desired $f = 0.5$. If the effective gap size (transit time) is not thin (short) compared to the initial bunch length L_b (pulse length t_p), beam particles experience too much of the $V(t)$ and a substantially reduced effective tilt f^* is achieved instead of the intended f . Longer t_p result in greater f^* , but at the cost of more longitudinal focusing aberration due to beam temperature over the longer drift length L_d (even hypothetical $T_b = 0$ eV beams acquire effective $T_{||}$ due to gap effects, as discussed below). As shown in Fig. 2, the extra voltage in the “smooth” $V(t)$ repopulates some of the head and tail of the velocity tilt with the excess beam, and the “smooth” waveform results in an increased compression ratio of 2650 with $t_{fwhm} = 0.035$ ns. The effective f^* are 0.3 and 0.4 for the “sharp” and “smooth” waveforms, respectively.

The transverse and longitudinal phase space of the beam are coupled within the gap because of the particle transit time compared to the temporal change in $V(t)$. An imbalance in the integrated radial electric field E_r is experienced by each particle, and radial movement with the gap implies an integrated axial electric field E_z imbalance as well, which is dependent upon the particle radius entering the gap. For $V(t) > 0$, particles at larger r encounter more decelerating E_z field, whereas the same receive more acceleration for $V(t) < 0$. As shown in Fig. 3, an initially cold beam gains velocity spread akin to an effective longitudinal temperature $T_{||}$ from the acceleration gap effects, and the associated chromatic aberration sets a finite upper bound on the compression. The case achieving the intended $f = 0.5$ across an infinitely thin gap is provided in Fig. 3 for comparison.

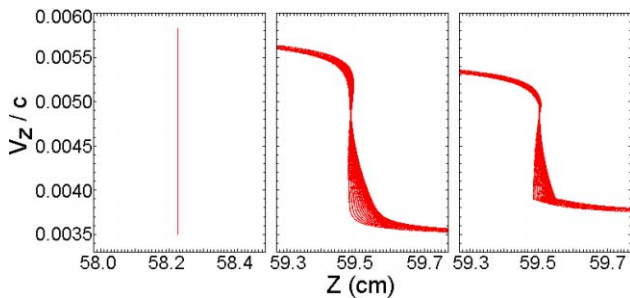


Fig. 3. $\{z, v_z\}$ phase space at the focal plane for the $T_b = 0$ eV beam using the “sharp” $V(t)$ across an infinitely thin gap (left), and “smooth” (center) and “sharp” (right) $V(t)$ waveforms across the finite-size gap.

Realizable beams necessarily have non-zero initial temperature, in addition to the effective temperature acquired by the gap and waveform. The focal plane becomes smeared because of the axial velocity spread, implying an increased axial tolerance for diagnostic and target alignment, but accompanied by a reduced peak compression that varies less sensitively as a function of z . Therefore, the initial $T_{||}$ of the beam further reduces the upper limit on axial compression by increasing the amount of aberration of the focal plane. In addition, slower head particles contribute more pre-pulse (post-

pulse) current upstream (downstream) of the focal plane, relative to the faster tail particles, since the slower particles suffer more aberration because the thermal velocity v_{th} of the beam is a greater fraction of the head velocity v_h than the tail velocity v_t . Faster tail particles are reduced from the intended maximum v_t more than slower head particles are increased from their intended minimum v_h . Since the energy modulation from $V(t)$ is not imparted instantaneously, accelerated particles have reduced transit times across the acceleration gap and their integrated energy gain is not equal and opposite to the deceleration of the slower particles.

The simulations discussed earlier are repeated with an initial beam temperature of $T_b = 0.2$ eV, which is in agreement with measurements in the NDCX device, and the results are provided in Fig. 4. As before, the “smooth” $V(t)$ effectively compresses more of the charge bunch relative to the “sharp” case, due to the excess voltage and larger achieved f^* , however, neither results in the compression associated with the intended $f = 0.5$ that the infinitely thin gap case achieves (also shown in Fig. 4). The compression ratios and t_{fwhm} for the three cases are approximately 400, 320, and 235, and 0.6 ns, 0.7 ns, and 0.65 ns, respectively. The differences between the cases are due to the decreased f^* relative to the intended value, which are interpreted as increases in effective $T_{||}$, since the compression is degraded without changing the location of the focal plane according to the equation given earlier for L_d , which nominally depends on f .

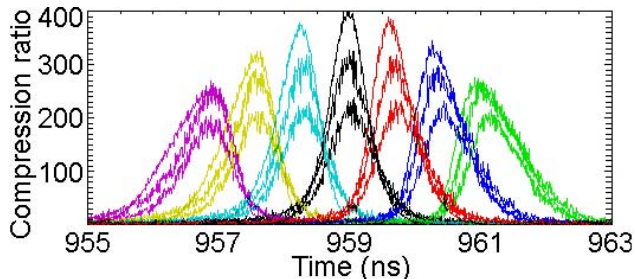


Fig. 4. Compression ratio comparison between “smooth” (middle profiles) and “sharp” (bottom profiles) $V(t)$ at multiple axial locations about the focal plane, in steps of $\Delta z = 0.1$ cm. The initialized $T_b = 0.2$ eV beams are velocity-tilted across the 3 cm gap. The results using the infinitely thin gap are provided as well (top profiles).

Additional simulations are executed for various initial T_b , from 0.1 eV to 1.6 eV, using the “smooth” waveform across the 3 cm gap, in order to investigate the dependence of the longitudinal compression on the initial emittance of the charge bunch. As evident in Fig. 5, the compression ratio decreases and the t_{fwhm} increases with an approximate square root dependence on T_b . When the voltage waveform accuracy and plasma neutralization levels are each very high in experiments, the maximum compression and minimum t_{fwhm} achieved at the focal plane will be emittance-dominated.

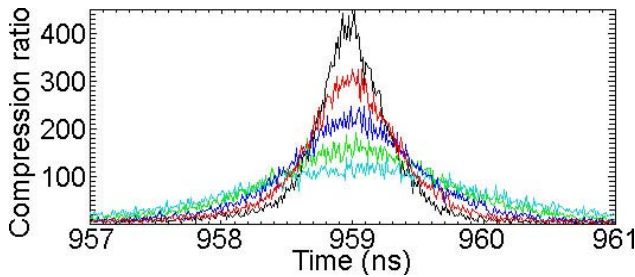


Fig. 5. Compression ratio comparison at the focal plane for initialized $T_b = 0.1$ eV (black), 0.2 eV (red), 0.4 eV (dark blue), 0.8 eV (green), and 1.6 eV (light blue).

The amount of effective longitudinal temperature imparted to an $E_0 = 400$ keV K^+ beam with non-zero initial T_b as it encounters the “smooth” waveform for $t_p = 300$ ns and $f = 0.5$ across the 3 cm gap can be determined by comparing to the case of an infinitely thin gap. Simulations of cases involving the same initial T_b , comparing the finite-size gap to the infinitely thin gap reveal an approximate 20% relative difference in compression ratio and t_{fwhm} . The effective $T_{||}$ difference for the 3 cm gap case, due to the reduced f^* from acceleration gap effects, is determined to be the equivalent of an approximately 45% increase from the initial T_b , for the parameters considered here.

TRANSVERSE DEFOCUSING EFFECT OF THE ACCELERATION GAP

In addition to the effective $T_{||}$ increase and reduced f^* caused by the acceleration gap, the E_r imbalance (mentioned earlier) across the gap provides an average time-dependent radial defocusing force to all portions of the beam during the compressing [$dV(t)/dt < 0$] part of the waveform, as shown in Fig. 6. Particles crossing the gap early in time [when $V(t) > 0$] sample more integrated $+E_r$ at the entrance compared to the exit, whereas particles crossing the gap late in time [when $V(t) < 0$] sample more integrated $+E_r$ at the exit compared to the entrance. In the center and right frames of the figure, electric field vectors are plotted and the black arrows indicating particle velocity vectors are exaggerated. The net effect is that all beam particles entering the gap intending to participate in the axial velocity tilt will receive a net divergence to their trajectories in a time-dependent manner.

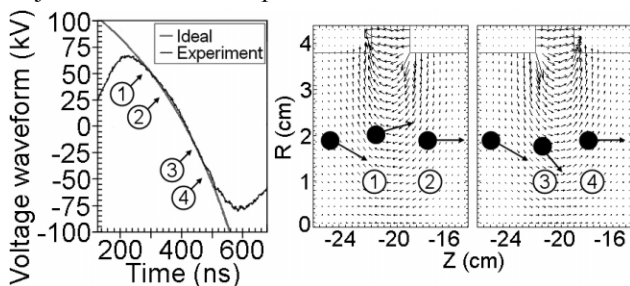


Fig. 6. Illustration of the radial defocusing effect of the gap during the $dV(t)/dt < 0$ portion of the waveform.

The time-dependent transverse defocusing effect in the NDCX device is witnessed both in simulations [12,13,15] and measurements [7]. Large spot sizes are unusable for target heating experiments since the current density (and energy deposition capability) of the beam is inversely proportional to the square of the radius at the focal plane. The simplest compensation method is to transversely “over-focus” the beam, whereby the charge bunch is given too large a radial convergence angle by the final transport magnet, such that the transverse defocusing effect of the acceleration gap balances the excess convergence in an average way, and recovers the originally intended convergence angle necessary to achieve simultaneous compression to a final focal-plane radius r_b^{foc} of 1-2 mm. Using the same modest NDCX-relevant parameters, simulations [12] demonstrate the beam density at the simultaneous focal plane for the nominal case to be 1.4×10^9 cm^{-3} , compared to 2.3×10^{11} cm^{-3} in the over-focused case (wherein the initial convergence angle is approximately doubled) due to the substantial difference in radius achieved at the focal plane (2 cm compared to 0.125 cm). The over-focusing technique is successfully employed in experiments [16], as shown in Fig. 7, and is required in order to recover sufficient main-pulse contrast, wherein the majority of the energy deposition of the beam resides within the longitudinally compressed beam current and helps reduce the associated target pre-heat by the pre-pulse, which is deleteriously large in the nominal cases without an excess initial convergence entering the acceleration gap.

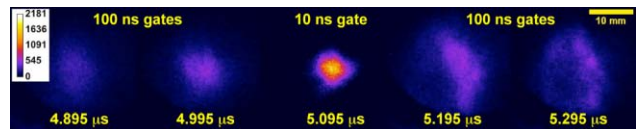


Fig. 7. Optical transverse scintillator images in a time-delayed sequence from over-focusing experiments in the NDCX device [16]. The high-intensity spot shows a minimum rms radius of approximately 2 mm at the time of peak longitudinal compression.

SIMULTANEOUS COMPRESSION USING A STRONG FINAL-FOCUS SOLENOID

Another method for achieving simultaneous transverse and longitudinal current density compression in spot sizes of a few mm or less, and in pulse durations of a few ns, is to employ a strong final-focus solenoid [5,12,13]. The range of on-axis solenoidal magnetic field magnitudes presently under consideration for charge bunch compression experiments is $B_z = 30$ -150 kG. Such a solenoid transversely re-focuses the longitudinally compressing beam (which is defocused by the acceleration gap), controls the transverse focal length, and reduces the amount of plasma density needed upstream to neutralize the beam (since the beam radius and density may remain larger and lower, respectively, throughout the drift region). Depending on the strength of the longitudinal and transverse focusing elements, total beam

current density compression factors between 10^3 and over 10^6 are expected when using a final-focus solenoid, largely due to the small focal plane beam radii achieved under optimized conditions (between ~ 0.01 - 1 mm) [12,13]. The amount of transverse compression sensitively depends on the solenoidal magnetic field magnitude, as well as its positioning relative to the simultaneous focal plane [5]. However, an axial velocity tilt contributes to transverse focusing aberration because the lower-energy beam head nominally focuses earlier in space and time relative to the higher-energy beam tail. The solenoid also results in longitudinal focusing aberration since beam particles entering the solenoid at the same axial coordinate z (and energy E_b), but at larger radius r , acquire more v_θ rotation due to the spatial dependence of the $B_z(r)$ field, and therefore will not focus at the exact same intended location because of the variation in applied radial focusing (according to the Lorentz force from v_θ and B_z).

In order to partially-fill the high-field region of the strong solenoid with sufficiently dense plasma for beam neutralization, supersonic cathodic-arc plasma will be injected upstream into the solenoid from off-axis filter coils located at the downstream end of the device (near the focal plane) [5]. Magnetic mirroring of the plasma away from the high-field region is the major concern, since simulations show stagnation of the simultaneously compressing beam in the presence of plasma whose density is only equal to (or less than) the expected peak beam density. Large-space-scale and long-time-scale 3D plasma flow simulations [17] demonstrate that high density plasma is expected to penetrate into the strong solenoid, largely due to the supersonic nature of the injected plasma, and result in significant plasma density compression along field lines. The plasma fill dynamics are sensitive to the magnetic topology created by the magnetized filter coils, as well as both the main and fringe fields of the final-focus solenoid. Recent experiments [18] have verified the compression of the plasma density as it flows along field lines towards the on-axis high-field region, as well as plasma penetration into and beyond the solenoid. A preliminary comparison between simulation and experiment of simultaneous transverse and longitudinal ion beam compression involving a recently constructed 80 kG final-focus solenoid (operating at 50 kG in the figure) is provided in Fig. 8.

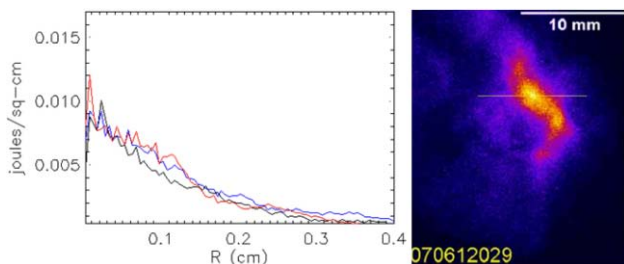


Fig. 8. Preliminary simulations (left) of simultaneous ion beam focusing, using a final-focus solenoid and realistic plasma flow profiles near the focal plane, predict an

approximate full-width, half-maximum beam radius of ~ 2 mm, in qualitative agreement with preliminary optical measurements [18] using a transverse scintillator (right).

SUMMARY

In order to achieve high intensities on target with space-charge-dominated beams for warm dense matter and heavy ion fusion applications, plasma neutralization-assisted focusing is required. Longitudinal bunch compression in the laboratory is constrained by acceleration gap size, voltage waveform shape and accuracy, beam temperature, initial pulse length, intended fractional tilt, and energy accuracy for the specified waveform. The over-focusing technique may be used to recover beam radii of a few mm at the focal plane by offsetting the time-dependent transverse defocusing effect, which is an inherent side-effect of the longitudinal focusing process. Simulations show total current density compression factors from 10^3 to over 10^6 may be achieved during final charge bunch focusing, depending on the strength and focal length of the focusing elements. Strong final-focus solenoids can be used for extreme simultaneous ion beam compression, and high-density supersonic plasma has been simulated and measured to partially penetrate such solenoids for beam neutralization.

REFERENCES

- [1] S. S. Yu, et. al., Fusion Sci. Technol. **44**, 266 (2003).
- [2] B. G. Logan, et. al., Nucl. Fusion **45**, 131 (2004).
- [3] D. A. Callahan, Fusion Eng. Des. **32-3**, 441 (1996).
- [4] B. G. Logan and D. A. Callahan, Nucl. Instrum. Meth. Phys. Res. A **415**, 468 (1998).
- [5] A. B. Sefkow, et. al., Nucl. Instrum. Meth. Phys. Res. A **577**, 289 (2007).
- [6] E. Henestroza, et. al., Phys. Rev. ST Accel. Beams **7**, 083501 (2004).
- [7] P. K. Roy, et. al., Phys. Rev. Lett. **95**, 234801 (2005).
- [8] A. B. Sefkow, et. al., Phys. Rev. ST Accel. Beams **9**, 052801 (2006).
- [9] A. B. Sefkow and R. C. Davidson, Phys. Rev. ST Accel. Beams **9**, 090101 (2006).
- [10] P. A. Seidl, et. al., Nucl. Instrum. Meth. Phys. Res. A **577**, 215 (2007).
- [11] E. Henestroza, private communication (2005).
- [12] A. B. Sefkow and R. C. Davidson, Phys. Rev. ST Accel. Beams **10**, submitted (2007).
- [13] A. B. Sefkow, Ph.D. Thesis, Princeton University (2007).
- [14] LSP is a software product of ATK Mission Research, Albuquerque, NM 87110.
- [15] C. H. Thoma, et. al., IEEE Proceedings of the 2005 Particle Accelerator Conference, 4006 (2005).
- [16] J. E. Coleman, et. al., IEEE Proceedings of the 2007 Particle Accelerator Conference, submitted (2007).
- [17] A. B. Sefkow, et. al., Phys. Rev. ST Accel. Beams **10**, submitted (2007).
- [18] P. K. Roy, et. al., IEEE Proceedings of the 2007 Particle Accelerator Conference, submitted (2007).